Thermochimica Acta, 212 (1992) 227–242
Elsevier Science Publishers B.V., Amsterdam

Thermomechanical analysis and viscometric properties of motor oils at low temperature [1]

Alan T. Riga

Lubrizol Corporation, 29400 Lakeland Blvd., Wickliffe, OH 44092 (USA)

(Received 2 January 1992; accepted 25 July 1992)

Abstract

Pumpability related engine failures have resulted from an inadequate understanding of the time-dependent rheology of motor oils at low temperatures. The current work elucidates the nature of the wax–oil structure formed at temperatures below the cloud points for a series of mineral oils and formulated lubricants having documented field and bench test performance. Low-temperature field performance of motor oils was differentiated by slow cool, low shear rate methods. The solidification of each motor oil was characterized by a viscosity–temperature profile. The activation energies for crystallization and fusion were higher for the problem oils. The creep moduli of wax–oil gels were determined from low temperature isothermal thermomechanical (TMA) experiments. The engine-pass oils had lower moduli at −65°C.

INTRODUCTION

The low-temperature operating limit of engine oils is dependent upon the flow characteristics of the lubricant. The capability off mineral oil lubricants to flow at low temperature is a function not only of viscosity but also of the precipitation of less soluble, waxy components. Relatively small amounts of wax can, under the proper cooling conditions, completely immobilize the bulk oil through formation of a three-dimensional network of interlocking crystals [1–8].

Many investigators have studied the pour point phenomenon, but the precise mechanism by which pour point depressants function is still not completely understood [1–8]. It is generally believed that the pour point depressant (PPD) inhibits crystal growth either by adsorption on the newly formed wax crystals or by cocrystallization with the wax. The actual process may be one or both, depending, upon the cooling rate and the chemical

Correspondence to: A.T. Riga, Lubrizol Corporation, 29400 Lakeland Blvd., Wickliffe, OH 44092, USA.

[1] Presented at the 20th Annual NATAS Conference, Minneapolis, MN, 20–26 September 1991.

nature of the PPD. Although the use of PPDs has been widespread in the manufacture of multi-grade motor oils, engine failures have resulted from an inadequate understanding of the time-dependent rheology of motor oils at low temperatures [1,9–16]. Gel formation can be attributed to solidification of the waxy components and the structural integrity of the wax–oil composite. Differentiation by "hard" gelation and "limited" gelation has been made by Selby [17] with a scanning viscometric technique that relates the rate of change of viscosity to temperature upon slow cooling. The hard gel is considered to be of high structural strength and the limited gel of lower strength.

Examination of the factors affecting the structure–property–performance relationship must continue to avoid future pumpability problems. The present work was undertaken to develop new low-temperature techniques to relate oil gelation phenomena to field performance. This study reports viscometric data from a number of commercially available slow cool, low shear rate methods which correlate with engine field service [17]. In addition, thermomechanical analysis (TMA) is introduced to define the solid state mechanical properties of the wax–oil composite structure formed upon cooling below the cloud point. Information on the flow characteristics of lubricants at the solid–liquid phase transition is presented.

EXPERIMENTAL

Lubricants

The lubricant samples used in this study included a Mid-Continent 100 solvent neutral mineral oil (SN) and eight ASTM pumpability reference oils (PROs). The mineral oil was studied with and without a commercial pour point depressant. The eleven lubricants are listed in Table 1. The PROs were chosen for their documented engine performance in the Border Line Pumping Temperatures test [18]. The viscometric properties of the mineral oil samples are given in Table 2. PRO engine performance is summarized in Table 3.

Viscosity measurements

All samples were heated at 80°C for 1 h then allowed to cool to room temperature before exposure to low temperatures. Samples for thermomechanical analysis (TMA) and differential scanning calorimetry (DSC) were prepared by cooling 25 to 50 mg at 0.10°C h^{-1} to −35°C. Samples were transferred to a −50°C bath for storage, then cooled to dry ice temperature before analysis.

A thermal analysis system with a thermal mechanical analyzer module [19] and a dual sample differential scanning calorimetry unit [20] was used to determine the melt-transition properties of pre-cooled samples.

TABLE 1

Materials studied by viscometric and mechanical methods

Sample	Identity	SAE grade	Description
A1	PRO-05 ASTM	10W40	Engine pumpability fail oil
A2	PRO-09 ASTM	10W40	Engine pumpability pass oil
A3	PRO-11 ASTM	10W40	Engine pumpability pass oil
A4	PRO-13 ASTM	10W40	Engine pumpability pass oil
A5	PRO-15 ASTM	10W	Engine pumpability pass oil
A6	PRO-16 ASTM	20W	Engine pumpability fail oil
A7	PRO-21 ASTM	10W30	Engine pumpability fail oil
A8	PRO-24 ASTM	10W40	Engine pumpability fail oil
B1	100 SN		100 solvent neutral oil
B2	100 SN + 0.10 wt% PPD		Item B1 plus a commercial pour point depressant additive
B3	100 SN + 0.50 wt% PPD		

The viscometric properties of the oils were determined by classical and several new techniques. The standard viscosity tests included ASTM D 97 (pour point), minirotary viscometry (MRV), ASTM D 3829 (47-h slow cool MRV TP1), and stable pour point (Federal 203, cycle C).

A commercial rotational viscometer was used to characterize the oils at low temperature. Samples were cooled at 0.01°C min^{-1} from 0°C to a temperature at which the viscosity was greater than 500 000 mPa s (1 mPa s = 1 cP). Shear stress was continuously monitored at a constant shear rate of 0.7 s^{-1}.

A scanning viscometric technique was also used to characterize the PRO samples.

ASTM D 5133 was used to characterize the oil viscosity. Samples were cooled at 1°C min^{-1} from room temperature until the viscosity exceeded 40 Pa s. The viscosity of the sample was monitored as a function of temperature. The temperature registered at a sample viscosity of 40 Pa s is defined as the critical pumpability temperature (CPT).

Thermomechanical analysis (TMA)

The TMA module was operated in the penetration mode using a 0.635 mm diameter flat-tipped needle probe. The solidified wax–oil composite tested was approximately 4.0 mm in diameter and 0.1 mm in height. When the sample was examined under load, the applied stress could be varied up to 2.45×10^6 Pa with a maximum load of 100 g. The probe was first zeroed on the bottom of an empty aluminum pan. The height of the frozen sample was determined by placing the probe without a load on the top of the solidified sample. Any displacement from the original height by expansion

TABLE 2

Viscometric properties of 100 SN with and without PPD

Sample	PPD concentration in 100 SN (wt%)	Pour point ASTM D97 temp. (°C)	Stable pour point Federal 203k, cycle C temp. (°C)	Viscosity at $T = -25$°C			
				MRV D3829 (Pa s)	MRV TP1 (Pa s)	Haake viscometric	
						$T = -25$°C (Pa s)	Scanning borderline pumping temp. (°C)
B1	0.00	−15	−23	4.58	5.94	45	−23
B2	0.10	−22	≤ −42	2.68	2.94	18	−28
B3	0.50	−26	≤ −42	2.61	2.86	5.1	−37

TABLE 3

Engine and laboratory performance of pumpability reference oils

Sample	Identity	MRV TP1 D2 178 $T = -25°C$ [a] (Pa s)	MRV TP1 −25°C (Pa s) (*)	MRV D3829 −25°C [a] (Pa s)	Borderline pumping temperature		Engine performance pass/fail	Haake viscometrics (*)		Scanning Brookfield viscometrics (*)		John Deere JDQ 95 [f]
					MRV TP1 (°C) (*)	Seven-engine average [a] (°C)		Temp. [b] (°C)	Viscosity [c] (Pa s)	Temp. [b] (°C)	Viscosity [e] (Pa s)	(*) $T = -30°C$
A1	PRO-05	Solid	Solid	76	−12	−17.5	Fail	−14.2	255	−10.5	TVTM [a]	Solid
A2	PRO-09	13.4	12.0	13	−27	−26.5	Pass	−31.8	9.7	−30.0	15.5	22 mm
A3	PRO-11	8.6	8.7	7.5	−30	−30.5	Pass	−32.1	9.8	−28.0	17.5	18 s
A4	PRO-13	8.0	9.1	8.5	−31	−32	Pass	−29.7	15.1	−26.7	30.3	15 mm
A5	PRO-15	6.3	6.2	7.2	−35	−33	Pass	−37.8	7.2	−36.6	14.2	6 s
A6	PRO-16	32	33	32	−24	−23.5	Fail	−27.0	28.9	−26.4	33.9	25 mm
A7	PRO-21	Solid	Solid	28.7	−12	ND [g]	Fail [h]	−13.4	406	−13.1	TVTM	Solid
A8	PRO-24	756	Solid	34.8	−11	ND	Fail [h]	−10.8	525	−8.6	TVTM	Solid

(*) Indicates values determined in this study. [a] ASTM D02.07.OC/MRVTF, June 1985, Attachment No. 5; TP1 temperature profile in MRV. Repeatability; ±11.7% and reproducibility = ±17.5%. [b] Temperature at 40 Pa s; critical pumpability temperature. [c] Viscosity at −25°C. [d] TVTM = too viscous to measure. [e] Viscosity at −30°C. [f] JDQ flow properties: 14.5 day slow cool to −30°C; time (s) to 30 mm of flow or flow in mm in 30 s. [g] ND, not determined. [h] Fail, based on physical properties.

or penetration as sensed by the linear variable differential transformer (LVDT) was recorded as the dimensional change in μm. The pre-cooled samples were examined at a heating rate of 5°C m^{-1} under a very low load (0.10 g). Dimensional change as a function of temperature and the penetration rate were determined.

In the TMA isothermal mode, the pre-cooled sample was brought to a constant temperature below the pour point of the oil and held there for 1 h. The mechanical properties of the wax–oil gel were determined by applying a low load (1.0 g) and allowing the system to equilibrate until the displacement was constant or varying slowly. Then the TMA LVDT was shut off, the load was increased to 5.0 g, and the displacement was monitored until again constant. This sequence was repeated with increasing load four or five times per sample. The load versus displacement data (stress vs. strain) were recorded for each sample at three or four temperatures. The creep modulus (Pa) was defined as the slope of the stress versus strain curve in the initial, linear region.

The pre-cooled oil samples were also examined by DSC. The heating rate from −100°C through the melt-transition temperature was 5°C min^{-1}.

X-ray diffraction analysis (XRD)

The 100 SN oil with and without 0.50 wt% of PPD was examined by wide angle X-ray diffractometry. The samples were placed in a specially designed aluminum cell with a $0.025 \times 25 \times 75$ mm^3 Mylar window, cooled to −20°C and held there for 6 h, then cooled to −50°C for 48 h. The solidified wax–oil composites were then rapidly cooled to dry ice temperature and placed in the XRD unit. The samples were scanned with filtered Cu Kα radiation at a rate of 2° 2θ min^{-1} from 30 to 54°C. Sample temperature was maintained between −60 and −80°C. The crystalline structures of the waxes are stable over this 20°C temperature range.

RESULTS

100 SN oils

The influence of PPD on the flow characteristics of 100 SN oil can be seen in the viscometric data summarized in Table 2. The pour point, stable pour point, and scanning borderline pumping temperature (the temperature where the viscosity equals 30 Pa s) decrease with increasing PPD concentration. Similarly, the ASTM D3829 and TP1 MRV viscosities show marked differences between the 100 SN oil and the PPD-treated oils. For this system, the logarithm of the viscosity at −25°C varies inversely with PPD concentration, with a linear correlation coefficient (R^2) of 0.94.

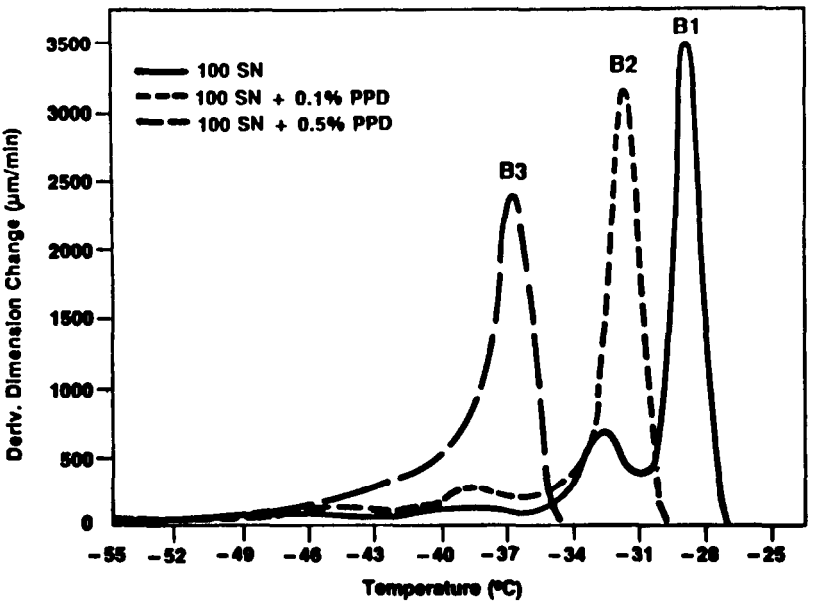

Fig. 1. Derivative TMA curve showing the effect of PPD the mechanical properties of 100 SN.

The TMA derivative curves of the 100 SN oils in Fig. 1 illustrate the effect of PPD on mechanical properties of 100 SN. The melt temperature (T_{ml}) and the maximum creep or strain rate (the peak value in derivative TMA) decrease with added PPD. Figure 2 shows the effect of increasing PPD concentration: the T_{ml} decreased, the scanning viscosity at -25°C decreased and the activation energy (E_a) diminished at the melt-transition temperature. The TMA activation energy is based on the creep rate, which is the rate of change of the thickness of the wax–oil composite at the onset of the melt-transition (Fig. 1). The logarithm of the creep rate versus the reciprocal absolute temperature is linear. The slope of this line is defined as the TMA activation energy at the melt-transition.

Pumpability reference oils (PROs)

Viscometric properties of the PRO samples with related field performance data are reported in Table 3. Linear relationships are observed between the ASTM seven-engine average borderline pumping temperature (BPT), the MRV TP1 BPT, and the scanning critical pumping temperature (CPT) at 40 Pa s, such that

Lab ASTM temperature = 8.71 + 1.30 (engine temperature)

or

MRV TP1 BPT (°C) = 8.71 + 1.30 (engine BPT (°C)) (1)

$R^2 = 0.93$ (see Fig. 3).

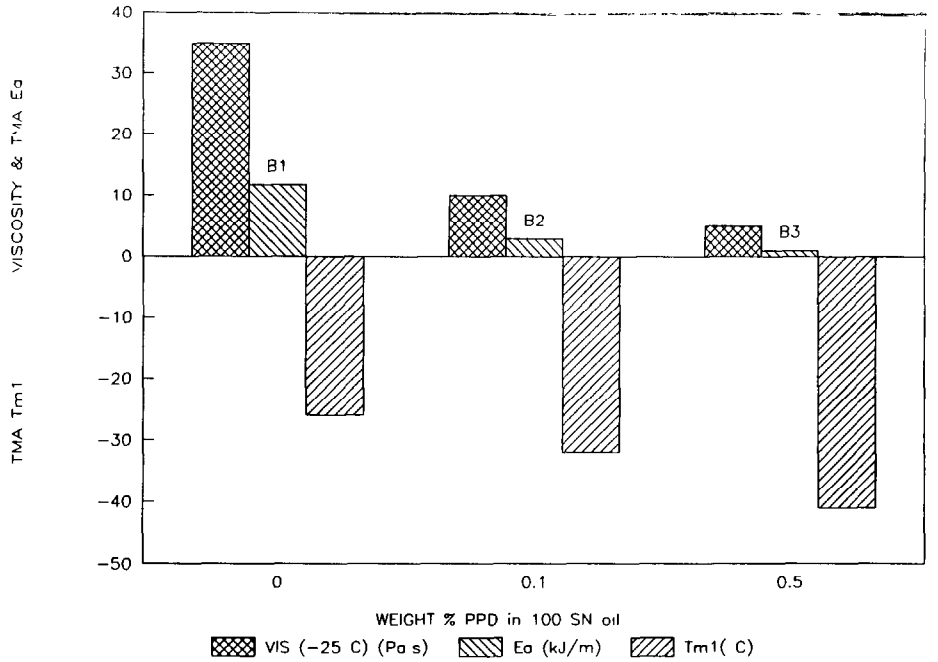

Fig. 2. Effect of PPD concentration on properties of 100 SN oil. The parameters for each sample are, from left to right, viscosity at −25°C (Pa s), E_a (kJ mol^{-1}) and T_{ml} (°C).

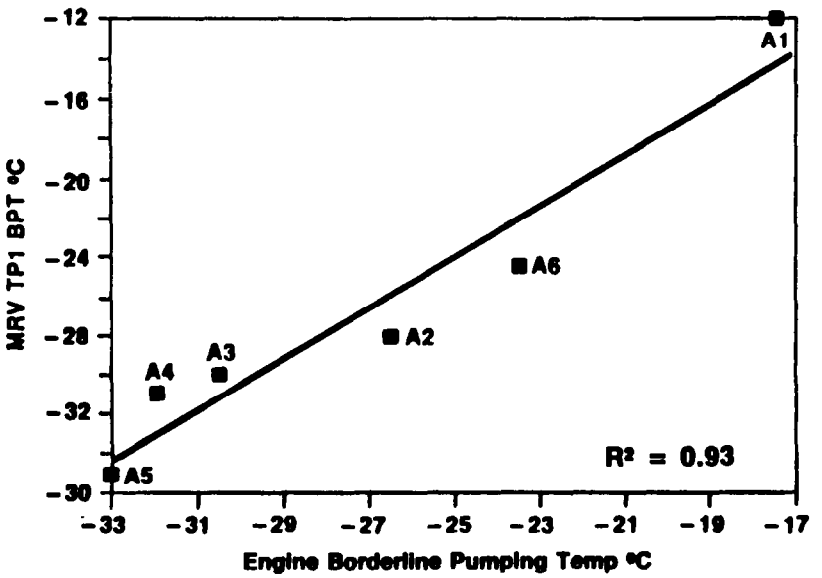

Fig. 3. Relationship between viscometric properties and borderline pumping temperature for PRO samples.

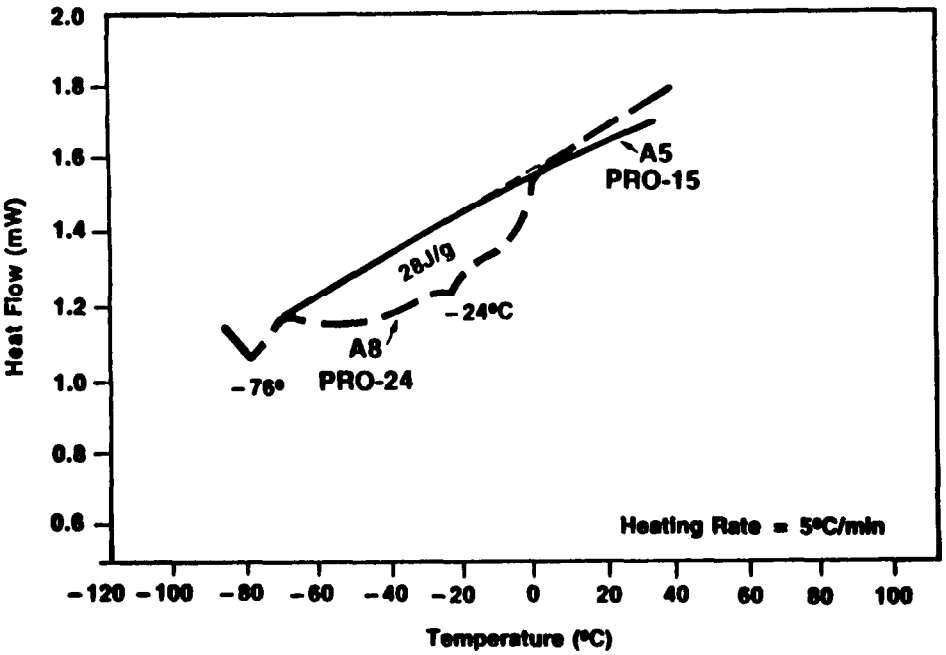

Fig. 4. DSC characteristics of samples A5 (PRO-15) and A8 (PRO-24); heating rate 5°C min^{-1}.

The scanning CPTs obtained by the previously discussed methods were in good agreement with BPT values, with a linear correlation coefficient of $R^2 = 0.96$.

Good correlations exist between engine performance (BPT) and the viscometric bench tests. The scanning viscosity varies linearly with the MRV TP1 viscosity at −25°C

Scanning lab viscosity = 4.33 − 0.687 (isothermal lab viscosity)

or

vis (Pa s) = 4.33 − 0.687 (MRV TP1 vis) (Pa s); $R^2 = 0.90$ (2)

The John Deere JDQ 95 flow characteristics at −30°C (See Table 3, last column) were also determined. The PROs were ranked in order of pass and fail from their physical properties.

PRO-15 and PRO-24 were characterized by TMA and DSC (Figs. 4 and 5). The fail oil, PRO-24, has a higher TMA melt-transition temperature regime than PRO-15 (−22 to −13°C) and exhibits endothermic heat flow from −70 to +10°C. The pass oil, PRO-15, has a lower TMA melt-transition temperature zone (−52 to −43°C) and no apparent heat flow in the temperature range −70 to +10°C. The TMA curves better differentiate the PRO samples than do the DSC curves because TMA is more sensitive

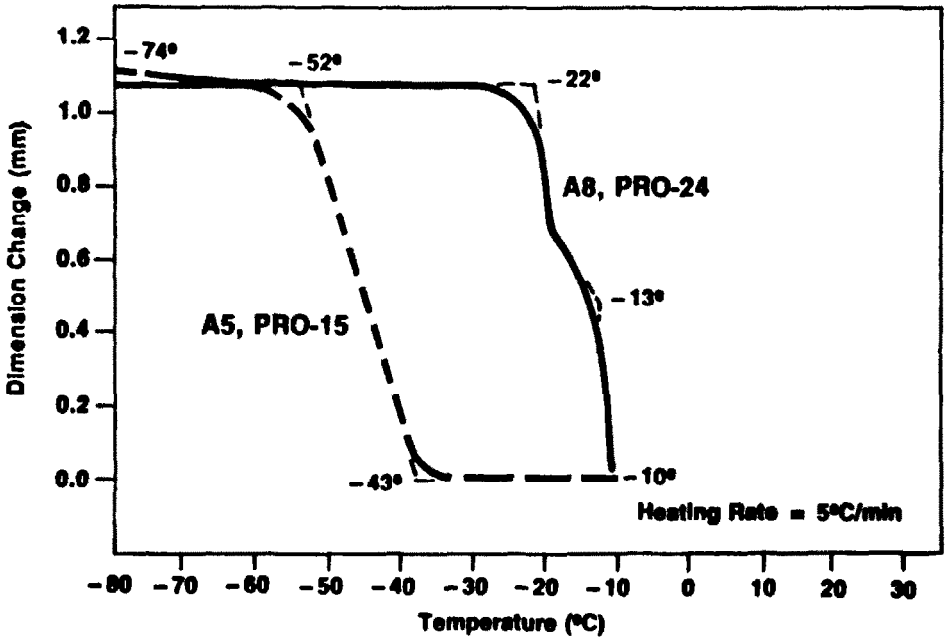

Fig. 5. TMA characteristics of samples A5 (PRO-15) and A8 (PRO-24); heating rate 5°C min^{-1}.

to solid state changes in the wax–oil composite during fusion. The heat of fusion of water is a considerable endothermic event masking a good deal of the DSC wax melting phenomenon. Moisture inadvertently introduced during sample preparation produces a minimal effect at 0°C in TMA. Therefore this study concentrated on the TMA properties of the wax–oil gels rather than the DSC heat flow properties.

The TMA melt-transition temperature (the extrapolated onset temperature for creep flow) did not separate the PROs based on BPT, CPT, or viscosity. The extreme cases of a good pumpability oil, PRO-15, and a poor pumpability oil, PRO-24, were distinguished.

The maximum creep or strain rate at the TMA melt-transition temperature (the peak in the derivative curve of penetration versus temperature) was found to be related to the seven-car average ASTM BPT (Fig. 6) with a linear correlation coefficient of $R^2 = 0.86$. Linear relationships were observed between the maximum creep rate and the MRV TP1 and the scanning viscosities [21] at −25°C.

The TMA activation energy at the onset of melting groups the PRO oils according to field performance. In Fig. 7 the average activation energy is 0.80 kJ m^{-1} for the pass PROs and 2.03 kJ m^{-1} for the fail PROs. The energy barrier for a solid wax network to be transformed to a liquid at the melt temperature is considerably lower for the good than for the poor field service oils.

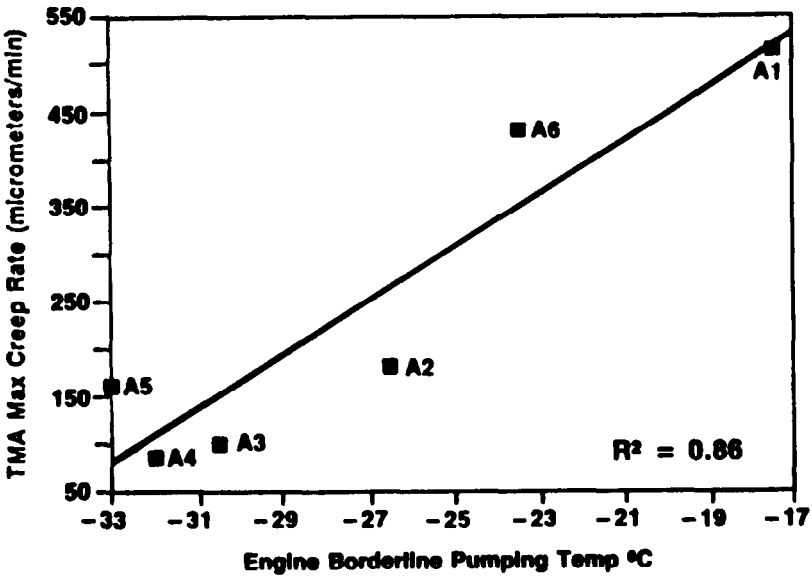

Fig. 6. Relationship of maximum creep rate at TMA melt-transition temperature to seven-engine average ASTM BPT.

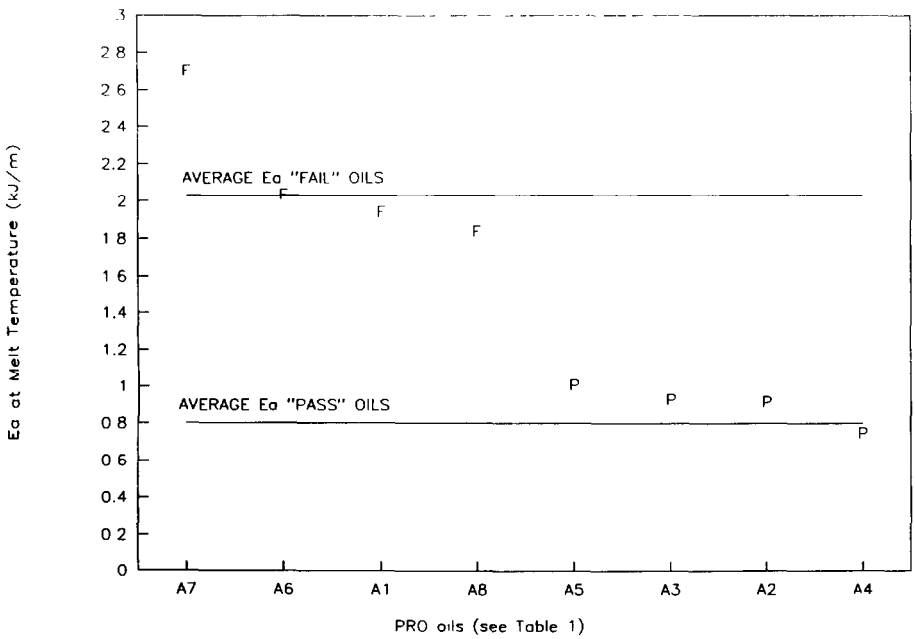

Fig. 7. TMA activation energy for PROs with poor (top line) and good (lower line) field performance.

TABLE 4

Activation energy for solidification of wax in PRO samples and 100 SN oils: activation energy from log viscosity vs. $1/T$ (K) curves [21]

Sample	Maximum activation energy (kJ m^{-1})	Sample	Maximum activation energy (kJ m^{-1})
A1	41.6	A5	5.2
A2	6.9	A6	5.4
A3	5.3	A7	41.8
A4	6.0	A8	38.2
B1	49.7		
B2	15.0		
B3	8.4		

Large activation energies for wax solidification were observed for poor pumpability oils (40.5 kJ m^{-1}) and lower values for good pumpability oils (5.7 kJ m^{-1}) (Table 4). This activation energy is a measure of the heat of crystallization of waxy components in the oil and of the viscosity increase of the amorphous phase. The addition of 0.5 wt% of a PPD effectively lowered the activation energy to less than one-fifth of the value for the non-treated oil.

The activation energy at the solidification-transition temperature for the PROs and 100 SN oils was calculated from scanning viscosity–temperature profiles (Fig. 8 and Table 4). The activation energy was taken at the

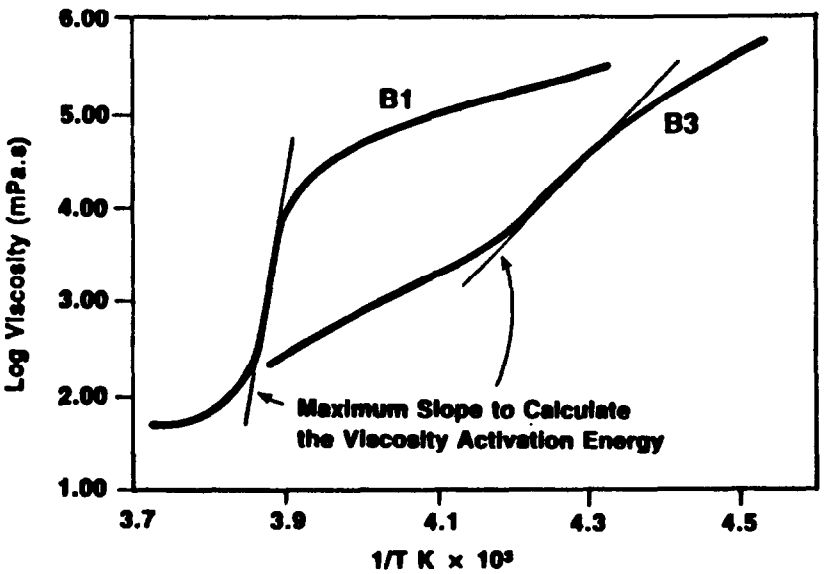

Fig. 8. Profile of Haake viscosity vs. reciprocal temperature.

TABLE 5

TMA creep modulus of pumpability reference oils and 100 SN oils

Sample	Engine pass/fail borderline pumping temperature	Creep modulus at $T = -65°C$ (Pa)
A5	Pass	1.1×10^5
A3	Pass	2.7×10^5
A7	Fail	8.5×10^6
A6	Fail	4.0×10^7
B3	Predicted pass	2.0×10^5
B1	Predicted fail	7.9×10^6

maximum slope in the log viscosity versus reciprocal absolute temperature curve [21]. The relative solidification (viscosity) activation energy for the two sets of oils studied indicates that the "good" oils have lower values than the "poor" oils. A high activation energy is the result of a rapid increase in viscosity over a narrow temperature range. The strength or hardness of the wax–oil composite at low temperature evaluated by the TMA creep modulus indicates that the "good" oils form "softer" gels (10^5 Pa) than the "poor" oils (10^7 Pa), as shown in Table 5.

DISCUSSION

Assuming that the mechanism for pour point depression is the adsorption of the chemical PPD on the crystal growth face, short stunted crystals should result (Figs. 9 and 10) [22]. The activation energy for the solid to liquid paraffin wax transition will be low for small, low aspect-ratio crystals. It will be high for well formed, high aspect-ratio interlocking crystal networks [18].

Interlocked wax networks would exhibit higher mechanical stiffness than the low aspect wax crystals. This is consistent with the isothermal TMA modulus results. That is, the interlocking paraffin crystal network produces harder gels (10^7 Pa) whereas the composite structure of PPD-treated oils yields softer gels (10^5 Pa).

The TMA activation energy is a measure of the mechanical driving force required to disturb the wax–oil network at the onset of melting. The TMA and viscosity activation energies of the PROs are clearly related to the pumpability of an oil at low temperatures. The average TMA activation energy for the pass PROs is 0.80 kJ m^{-1}, whereas the fail PROs have an average value of 2.03 kJ m^{-1} (Fig. 7). This TMA property separates the pass and fail samples into a "go" or "no-go" situation.

Thermal and mechanical changes occurring at the solid-to-liquid transition of two wax–oil systems have been studied. Differences in wax forma-

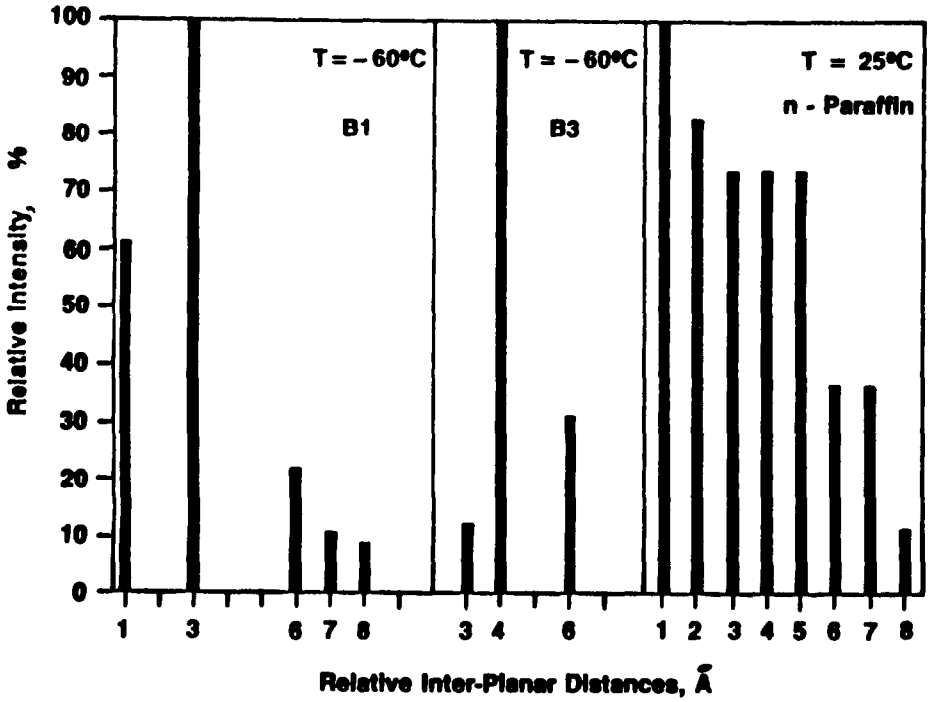

Fig. 9. Paraffin crystal structure of wax–oil systems at −60°C as shown by wide-angle X-ray diffraction.

tion of samples of 100 neutral mineral oil were observed in terms of the scanning borderline pumping temperature (at 30 Pa s) and the solidification activation energy. TMA yielded major differences at the wax melt which were related to the PPD concentration. These methods clearly demonstrate the effects of the addition of the PPD.

The paraffin crystal structure of waxy oil at −60°C was determined by wide-angle X-ray diffraction (Figure 9). The PPD caused a pronounced

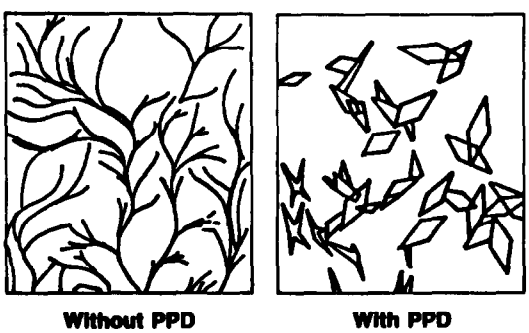

Fig. 10. Effect of pour point depressant on crystal morphology of wax in a lubricating oil.

change in the crystal morphology and crystal growth habit of the waxy. McCrone reported that the length-to-diameter ratio of waxy crystals in a PPD-treated oil decreased with increasing concentration of the additive from 150 to about 10 [22]. In a qualitative sense, McCrone's observations agree with the X-ray diffraction results.

The Arrhenius activation energy for solidification (cooling cycle) of the wax–oil composite was derived from the logarithm of the viscosity versus the reciprocal absolute temperature. The addition of 0.5 wt% of a PPD effectively lowered the activation energy for crystallization of the wax by 17% of the untreated value (Table 4, B1 vs. B3).

CONCLUSIONS

This study has explored several new techniques to elucidate pumpability phenomena. PPD-treated oil forms wax crystals that lead to a low modulus wax–oil composite. This softer gel melts at a lower temperature than the harder gel in the untreated oil, has a lower mechanical activation energy and is formed with lower viscometric activation energy. The TMA and viscometric properties have been clearly related to the low-temperature performance of the lubricants.

ACKNOWLEDGMENTS

The author thanks Frank Abbott, Dr. S. Baczek (Dylon Inc.), Dr. Michael Covitch and Ted Selby (Savant Inc.) for their helpful discussions and information. Thanks also go to Darryl Gundic and Elizabeth Sumiejski for assisting in the thermal and viscometric analysis.

REFERENCES

1 G.M. Schmidt, M.T. Olsen and M.I. Michael, Low Temperature Fluidity of Lubricating Oils under Slow Cool Conditions, SAE Tech. Pap. Ser., No. 831718.
2 R.H. Johnson and C.E. Kelly, Effect of Additives on Low-Temperature Viscometric Properties of SAE 5W-30 Engine Oils, Natl. Pet. Refiners Assoc., [Tech. Pap.], FL-83-87 (1983) 1.
3 S.G. Agaev, L.P. Kazakova, A.A. Gundyrev and N.V. Sidorova, Electrokinetic studies of mechanism of pour point depressant action, Khim. Tekhnol. Topl. Masel, (9) (1980) 40.
4 G. Gavlin, E.A. Swire and S.P. Jones, Pour point depression of lubricating oils, Ind. Eng. Chem., 45 (1953) 2327.
5 C.E. Hodges and D.T. Rogers, Some new aspects of pour-depressant treated oils, Oil Gas J., (Oct.), (1947) 89.
6 G.A. Holder and J. Winkler, Mechanism of pour depression in distillate oils, Symposium on Additives in the Petroleum Industry, ACS Meeting, April 1965, pp. D49–D64.
7 Petroleum additives—pour point depressants, Encyl. Polym. Sci. Technol., 9 (1968) 843.
8 J.G. McNab, D.T. Rogers, A.E. Michaels and C.E. Hodges, Pour-point stability characteristics of winter-grade motor oils, SAE Q. Trans., 2 (1) (1948) 34.

9 R.L. Stambaugh, Engine oil viscosity classification task force low temperature report, Attached to Minutes of SAE Subcommittee 2 Meeting, June 9, 1981.
10 R.S. Johnson, A Laboratory Engine Test Study of Motor Oil Flow Properties in Winter Service, SAE Tech. Pap. Ser., No. 841387.
11 A. Rossi, Wax and Low Temperature Engine Oil Pumpability, SAE Tech. Pap. Ser., No. 852113.
12 R.L. Stambaugh and J.H. O'Mara, Low temperature flow properties of engine oils, SAE Trans., 91, SAE Tech. Pap. Ser., No. 821247.
13 J.E. Clevenger and H.F. Richards, Low Temperature Rheology of Multi grade Engine Oils—Formulary Effects, SAE Tech. Pap. Ser., No. 831716.
14 R.M. Stewart, M.F. Smith Jr., H. Shaub and T.W. Selby, Summary of ASTM Activities on Low Temperature Engine Oil Pumpability, SAE Tech. Pap. Ser., No. 821206.
15 R.L. Stambaugh, Low Temperature Pumpability of Engine Oils, SAE Tech. Pap. Ser., No. 841388.
16 H. Shaub and C.K. Murphy, Minirotary viscometer and engine oil pumpability, Lubr. Eng., 37 (1981) 377.
17 T.W. Selby, Further Considerations of Low-Temperature, Low-Shear Rheology Related to Engine Oil Pumpability. Information from the Scanning Brookfield Technique, SAE Tech. Pap. Ser., No. 852115.
18 ASTM D02.07.OC/MRVTF, Attachment 5, TP1 Temperature Profile in MRV, June, 1985.
19 A.T. Riga, Heat distortion and mechanical properties of polymers by thermal-mechanical analysis, Polym. Eng. Sci., 14 (1974) 764.
20 A.T. Riga, Inhibitor selection for vinyl monomers by differential scanning calorimetry, Polym. Eng. Sci., 16 (1976) 836.
21 J.R. Van Wazer, J.W. Lyons, K.Y. Kim and R.E. Colwell, Viscosity and Flow Measurements, Interscience, New York, 1963, p. 38.
22 W.C. McCrone, Study of pour-point depressants in lubricating oil, in Fusion Methods in Chemical Microscopy, Interscience, New York, 1956, pp. 189–191.